

## Electrical Conductance of Conjugated Oligomers at the Single Molecule Level

Roman Huber,<sup>†</sup> Maria Teresa González,<sup>†</sup> Songmei Wu,<sup>†</sup> Michael Langer,<sup>‡</sup>  
Sergio Grunder,<sup>‡</sup> Viviana Horhoiu,<sup>‡</sup> Marcel Mayor,<sup>‡,§</sup> Martin R. Bryce,<sup>||</sup>  
Changsheng Wang,<sup>||</sup> Rukiat Jitchati,<sup>||</sup> Christian Schönenberger,<sup>\*,†</sup> and  
Michel Calame<sup>\*,†</sup>

*Department of Physics, University of Basel, Klingelbergstrasse. 82, CH-4056 Basel, Switzerland,  
Department of Chemistry, University of Basel, St. Johanns-Ring 19, CH-4056 Basel,  
Switzerland, Forschungszentrum Karlsruhe GmbH, Institute for Nanotechnology, P.O. Box 3640,  
D-76021 Karlsruhe, Germany, and Department of Chemistry, University of Durham, Durham  
DH1 3LE, U.K.*

Received September 23, 2007; E-mail: christian.schoenenberger@unibas.ch; michel.calame@unibas.ch

**Abstract:** We determine and compare, at the single molecule level and under identical environmental conditions, the electrical conductance of four conjugated phenylene oligomers comprising terminal sulfur anchor groups with simple structural and conjugation variations. The comparison shows that the conductance of oligo(phenylene vinylene) (OPV) is slightly higher than that of oligo(phenylene ethynylene) (OPE). We find that solubilizing side groups do neither prevent the molecules from being anchored within a break junction nor noticeably influence the conductance value.

### Introduction

Major improvements in the assessment of charge transfer through a single-molecule have recently been achieved with reports that converge on the single-molecule conductance value for the simplest conceivable molecule, which is a short alkane chain anchored in between Au contacts via thiol terminals.<sup>1–6</sup> This important advance is based on the use of techniques with which the conductance of molecular junctions can be measured at the single molecule level.<sup>7–13</sup> This is in contrast to other

approaches where a single molecule conductance value is deduced from junctions encompassing few hundreds to several thousands of molecules.<sup>14–18</sup> In this case, one has to estimate the number of molecules in the junctions, which is prone to errors. While this achievement on alkanedithiols is a major step, molecular electronics focuses on conjugated molecules for which a similar agreement on single-molecule conductance values has not yet been reached. Of particular interest are molecular rods consisting of a conjugated backbone between terminal anchor groups allowing for immobilization in a junction. Prototype conjugated molecules of this kind are oligo(phenylene vinylene) and oligo(phenylene ethynylene) with sulfur anchoring groups for which we will be using the shorthand OPV and OPE in following.

There have been studies on self-assembled monolayers using scanning tunneling and atomic-force microscopy,<sup>19–21</sup> but most of the work on such kind of molecules has been done for relatively large-area junctions, realized for example by crossed-wires,<sup>22,23</sup> electrochemically grown nanowires,<sup>24,25</sup> nanopores,<sup>13</sup> and Au colloid arrays.<sup>26</sup> Only three studies of OPE compounds

- <sup>†</sup> Department of Physics, University of Basel.  
<sup>‡</sup> Department of Chemistry, University of Basel.  
<sup>§</sup> Institute for Nanotechnology.  
<sup>||</sup> University of Durham.
- (1) Li, X.; He, J.; Hihath, J.; Xu, B.; Lindsay, S. M.; Tao, N. J. *J. Am. Chem. Soc.* **2006**, *128*, 2135.
  - (2) Chen, F.; Li, X.; Hihath, J.; Huang, Z.; Tao, N. J. *J. Am. Chem. Soc.* **2006**, *128*, 15874.
  - (3) Li, Z.; Pobelov, I.; Han, B.; Wandlowski, T.; Blaszczyk, A.; Mayor, M. *Nanotechnology* **2007**, *18*, 044018.
  - (4) González, M. T.; Wu, S.; Huber, R.; van der Molen, S. J.; Schönenberger, C.; Calame, M. *Nano Lett.* **2006**, *6*, 2238.
  - (5) Suzuki, M.; Fujii, S.; Fujihira, M. *Jpn. J. Appl. Phys.* **2006**, *45*, 2041.
  - (6) Fujihira, M.; Suzuki, M.; Fujii, S.; Nishikawa, A. *Phys. Chem. Chem. Phys.* **2006**, *8*, 3876.
  - (7) Jang, S.-Y.; Reddy, P.; Majumdar, A.; Segalman, R. A. *Nano Lett.* **2006**, *6*, 2362.
  - (8) Bumm, L. A.; Arnold, J. J.; Cygan, M. T.; Dunbar, T. D.; Burgin, T. P.; Jones, L.; Allara, D. L.; Tour, J. M.; Weiss, P. S. *Science* **1996**, *271*, 1705.
  - (9) Reed, M. A.; Zhou, C.; Muller, C. J.; Burgin, T. P.; Tour, J. M. *Science* **1997**, *278*, 252.
  - (10) Kergueris, C.; Bourgoin, J.-P.; Palacin, S.; Fsteve, D.; Urbina, C.; Magoga, M.; Joachim, C. *Phys. Rev. B* **1999**, *59*, 12505.
  - (11) Cui, X. D.; Primak, A.; Zarate, X.; Torföhr, J.; Sankey, O. F.; Moore, A. L.; Moore, T. A.; Gust, D.; Harris, G.; Lindsay, S. M. *Science* **2001**, *294*, 571.
  - (12) Weber, H. B.; Reichert, J.; Weigend, F.; Ochs, R.; Beckmann, D.; Mayor, M.; Ahlrichs, R.; Löhneysen, H. *Chem. Phys.* **2002**, *281*, 113.
  - (13) Mantooth, B. A.; Weiss, P. S. *Proc. IEEE* **2003**, *91*, 1785.
  - (14) Chen, J.; Wang, W.; Reed, M. A.; Rawlett, A. M.; Price, D. W.; Tour, J. M. *Appl. Phys. Lett.* **2000**, *77*, 1224.

- (14) Kushmerick, J. G.; Holt, D. B.; Yang, J. C.; Naciri, J.; Moore, M. H.; Shashidhar, R. *Phys. Rev. Lett.* **2002**, *89*, 086802.
- (15) Rampi, M. A.; Whitesides, G. M. *Chem. Phys.* **2002**, *281*, 373.
- (16) Metzger, R. M. *J. Solid State Chem.* **2002**, *168*, 696.
- (17) Li, C.; Zhang, D.; Liu, X.; Han, S.; Tang, T.; Zhou, C.; Fan, W.; Koehne, J.; Jie Han.; Meyyappan, M.; Rawlett, A. M.; Price, D. W.; Tour, J. M. *Appl. Phys. Lett.* **2003**, *82*, 645.
- (18) Chen, Y.; Jung, G.-Y.; Ohlberg, D. A. A.; Li, X.; Stewart, D. R.; Jeppesen, J. O.; Nielsen, K. A.; Stoddart, J. F.; Williams, R. S. *Nanotechnology* **2003**, *14*, 462.
- (19) Rawlett, A. M.; Hopson, T. J.; Nagahara, L. A.; Tsui, R. K.; Ramachandran, G. K.; Lindsay, S. M. *Appl. Phys. Lett.* **2002**, *81*, 3043.
- (20) Blum, A. S.; Yang, J. C.; Shashidhar, R.; Ratna, B. *Appl. Phys. Lett.* **2003**, *82* (19), 3322.
- (21) Seferos, D. S.; Blum, A. S.; Kushmerick, J. G.; Bazan, G. C. *J. Am. Chem. Soc.* **2006**, *128*, 11260.

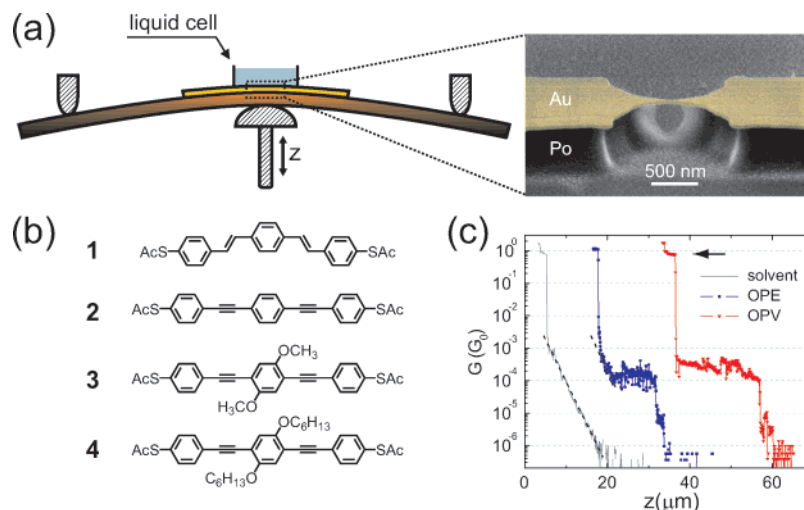


**Figure 1.** (a) Schematics of the MCBJ principle with a liquid cell and a SEM image of the central part of the microfabricated Au junction. (b) Structures of the molecules examined in this study: **1**, oligo(phenylene vinylene) (OPV) and **2–4**, oligo(phenylene ethynylene)s (OPEs). (c) Typical measurements of the electrical conductance  $G(z)$  as a function of pushrod movement  $z$  during an opening cycle in the pure solvent (gray) and in the same solvent to which conjugated OPE (blue) or OPV (red) molecules were added. The attenuation between the vertical pushrod movement  $\Delta z$  and the respective variation in the gap distance  $\Delta d$  is found in the range of  $a = \Delta d/\Delta z = (1.6\text{--}4) \times 10^{-5}$ .

could address single-molecule transport properties directly.<sup>27–29</sup> As a result, the absolute conductance values obtained for OPE and OPV compounds still span about 2 orders of magnitude. Previous work point to a higher conductance of OPV as compared to OPE,<sup>22–24</sup> but there also exists a large variation in the ratio, ranging from a factor of 2 to as much as 10.

In this letter we present quantitative measurements of the electrical conductance  $G$  of both OPE and OPV molecules using mechanically controllable break junctions (MCBJ) in a controlled liquid environment.<sup>30</sup> These measurements provide an assessment and a comparison of the single-molecule conductance values of OPE and OPV under identical conditions directly. We compare OPV with OPE and with two modified OPE's on which solubilizing side groups were added.<sup>31</sup> We find that OPV conducts better than OPE, but the difference is modest with typical conductance values of  $(2.0 \times 10^{-4})G_0$  and  $(1.2 \times 10^{-4})G_0$  ( $G_0 = 2e^2/h = 77.5 \mu\text{S}$ ) for OPV and OPE, respectively.

## Experimental

The principle of the mechanically controllable break junction (MCBJ) is sketched in Figure 1a. An actual device (sample) consists of a suspended Au bridge, typically  $0.1 \mu\text{m}$  in width and  $0.2\text{--}0.3 \mu\text{m}$  in

length, microfabricated on a flexible spring steel plate substrate, onto which a several  $\mu\text{m}$  thick insulating polyimide layer is cast. The metallic bridge is defined by electron-beam lithography on the substrate, followed by the evaporation of Ti (10 nm) and Au (60 nm), and is concluded after etching the polyimide in an oxygen plasma, thereby defining the suspended bridge. The sample is mounted in a mechanical bending apparatus: two counter supports hold the sample on the side, while a pushrod is pressing in the center from below ( $z$  movement), bending the substrate. Because of the bending, the Au bridge elongates and finally breaks in the narrowest section of the bridge when the strain exceeds the breaking strength. The resulting gap of size  $d$  can now be increased or decreased by moving the pushrod up or down. Most importantly, there is a large attenuation between the variation in the vertical pushrod movement  $\Delta z$  and the respective variation in the gap distance  $\Delta d$ . The attenuation factor<sup>30,32</sup> is found in the range of  $a = \Delta d/\Delta z = (1.6\text{--}4) \times 10^{-5}$ . The pushrod is driven via a micrometer screw and a gear-box by a stepper motor at a velocity of  $v_z = 30 \mu\text{m/s}$ , so that the two Au leads separate at  $0.5\text{--}2.0 \text{ nm/s}$ . In the following, we will also use the term “junction” for such a broken Au bridge and we will call it molecular junction if molecules are anchored in between the gap. The latter is achieved by adding molecules in solution to the junction area. We use a liquid cell which consists of a viton tubing gently pressing against the substrate from above.<sup>30</sup> To determine the (linear response) electrical conductance of a molecular junction, a (relatively small) voltage bias of  $0.2 \text{ V}$ <sup>33</sup> is applied between the left and right contact and the resulting current is measured with a custom-made current-to-voltage converter. This converter implements a fast automatic switching of the gain in between  $10^4$  and  $10^9 \text{ V/A}$  enables measurements of conductance values ranging over many orders of magnitude, from the quantized conductance value of a single atom contact  $G_0 = 2e^2/h$ <sup>34,35</sup> down to  $\sim 10^{-7}G_0$ .

To assess the conductance  $G$  of a particular molecule, the junction is periodically opened and closed in the presence of a  $0.25 \text{ mM}$  solution of molecules **1–4** (Figure 1b) in a mixture of THF/Mesitylene (1:4 v/v-ratio) (henceforth the solvent) to which  $15 \mu\text{M}$  tetrabutylammonium

- (22) Kushmerick, J. G.; Holt, D. B.; Pollack, S. K.; Rattner, M. A.; Yang, J. C.; Schull, T. L.; Naciri, J.; Moore, M. H.; Shashidhar, R. *J. Am. Chem. Soc.* **2002**, *124*, 10654.
- (23) Seferos, D. S.; Trammell, S. A.; Bazan, G. C.; Kushmerick, J. G. *Proc. Natl. Acad. Sci. U.S.A.* **2005**, *102*, 8821.
- (24) Cai, L. T.; Skulason, H.; Kushmerick, J. G.; Pollack, S. K.; Naciri, J.; Shashidhar, R.; Allara, D. L.; Mallouk, T. E.; Mayer, T. S. *J. Phys. Chem. B* **2004**, *108*, 2827.
- (25) Hassenkam, T.; Moth-Poulsen, K.; Stuhr-Hansen, N.; Nørgaard, K.; Kabir, M. S.; Bjørnholm, T. *Nano Lett.* **2004**, *4* (1), 19.
- (26) Liao, J.; Bernard, L.; Langer, M.; Schönenberger, C.; Calame, M. *Adv. Mater.* **2006**, *18*, 2444.
- (27) Reichert, J.; Ochs, R.; Beckmann, D.; Weber, H. B.; Mayor, M.; v. Löhneysen, H. *Phys. Rev. Lett.* **2002**, *88*, 176804.
- (28) Mayor, M.; Weber, H. B.; Reichert, J.; Eling, B.; v. Hänisch, C.; Beckmann, D.; Fischer, M.; Reichert, J.; Ochs, R.; Beckmann, D.; Weber, H. B.; Mayor, M.; v. Löhneysen, H. *Angew. Chem., Int. Ed.* **2003**, *42*, 5834.
- (29) Xiao, X.; Nagahara, L. A.; Rawlett, A. M.; Tao, N. J. *J. Am. Chem. Soc.* **2005**, *127*, 9235.
- (30) Gräter, L.; González, M. T.; Huber, R.; Calame, M.; Schönenberger, C. *Small* **2005**, *1*, 1067.
- (31) Haiss, W.; Wang, C.; Grace, I.; Batsanov, A. S.; Schiffrin, D. J.; Higgins, S. J.; Bryce, M. R.; Lambert, C. J.; Nichols, R. J. *Nat. Mater.* **2006**, *5*, 995.

- (32) Vrouwe, S. A. G.; van der Giessen, E.; van der Molen, S. J.; Dulic, D.; Trouwborst, M. L.; van Wees, B. J. *Phys. Rev. B* **2005**, *71*, 035313.
- (33) Note, that the current-voltage characteristic is linear in this low-voltage regime.
- (34) Scheer, E.; Agrait, N.; Cuevas, J. C.; Yeyati, A. L.; Ludoph, B.; Martín-Rodero, A.; Bollinger, G. R.; van Ruitenbeek, J. M.; Urbina, C. *Nature* **1998**, *394*, 154.
- (35) Agrait, N.; Levy-Yeyati, A.; van Ruitenbeek, J. M. *Phys. Rep.* **2003**, *377*, 81.

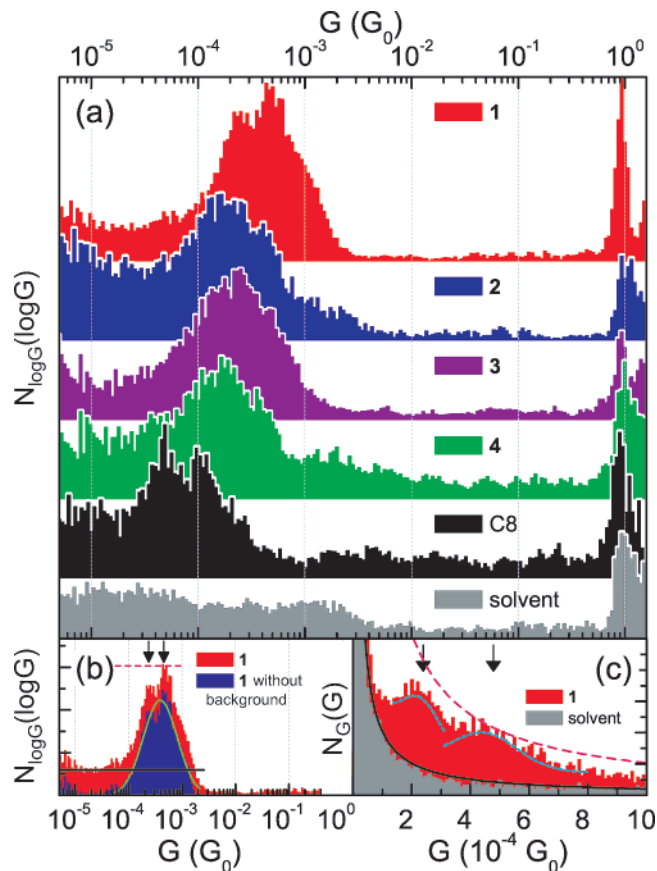
hydroxide (TBAH) was added to remove the acetyl protection groups *in-situ* in the liquid cell. During the measurements, the solution was kept under Ar atmosphere to prevent the deprotected bifunctional molecules from polymerization via disulfide bond formation. The junction is opened until the conductance value  $G$  is below the resolution limit and it is closed until a Au–Au contact is re-established, identified by  $G > G_0$  ( $\approx 10G_0$ ). During opening and closing,  $G$  is continuously recorded. In this work, 100 open-close cycles define one set of measurement. For all molecules at least three sets of measurements were taken, with each set acquired on a freshly prepared (virgin) sample which has not been broken before. A set of measurement is analyzed by plotting the conductance values  $G$ , or the logarithm of  $G$ , acquired during the opening phase in a histogram. To understand the histograms, we briefly emphasize the major characteristic features appearing in a single opening curve, in which  $G$  as a function of  $z$  is measured.

Figure 1c presents three  $\log G(z)$  curves, representative for the solvent alone (gray curve) and conjugated OPV/OPE molecules (green curves). After a plateau close to  $1 G_0$  (arrow) due to a final monatomic Au contact, the Au bridge breaks open, leading to a fast drop in  $G$ . This drop is due to a sudden retraction of the Au atoms. The gap then stabilizes between  $10^{-2}$  and  $10^{-3} G_0$  (depending on sample) after which a tunneling decay is observed (dashed line). This exponential decay with distance is the only feature present in the solvent (gray curve). In contrast, when conjugated molecules are present in solution, clear plateaus appear, signaling the presence of anchored molecules bridging the junction.

Individual conductance traces can vary quite a bit, from flat plateaus with different degrees of superimposed fluctuations, to inclined plateaus. They can exhibit strong switching noise and a plateau does not always show up, even in the presence of conjugated molecules. This is why a statistical analysis in the form of histograms is required to analyze the data.<sup>36,37</sup> In contrast to other groups, we find it more appropriate to discuss the measured  $G(z)$  values in a  $\log(G)$  representation, because only this representation is able to provide an overview of the junction conductance during the whole breaking process. Moreover, it is straightforward in the  $\log(G)$  representation to determine a pure tunneling background that can be subtracted without affecting the conclusion.<sup>4</sup> This is because a tunneling dependence in  $G(z)$  results in a constant contribution to the  $\log(G)$ -histogram, whereas a (noisy) plateau, as the ones shown in Figure 1c, produces a (broad) peak (see, e.g., Figure 2b), which we identify as the signature of the anchored conjugated molecules. The width of this peak reflects the fluctuations in the molecular junctions, caused for example by the switching of the molecules between different binding sites (hollow, on-top, or bridge site).<sup>1,5</sup> As we will show below, the peaks in the  $\log G$ -histogram appear to be surprisingly symmetric, suggesting that the fluctuations are approximately Gaussian around a central value in the log-representation.

## Results

Figure 2 shows a set of representative conductance histograms measured for molecules 1–4. These are compared with histograms obtained for two references, which are octanedithiol molecules ( $C_8$ ) in mesitylene and the solvent alone. Figure 2a emphasizes on the comparison using a  $\log(G)$  representation. In contrast to the solvent, there appear pronounced, nearly symmetric peaks on a relatively flat background in a conductance window around  $10^{-4}G_0$  to  $10^{-3}G_0$  for  $C_8$  and 1–4. These peaks are the signature of molecules that are trapped in atomic-sized junctions. Focusing on the central weight of each peak, we see that molecule 1 (OPV) conducts best, followed by molecules 2–4 (OPEs). In contrast, the reference compound  $C_8$  has clearly a lower conductance value. Taking different



**Figure 2.** (a) Log-histograms of measured conductance values  $\log(G)$  obtained during one hundred successive open cycles similar to those three examples shown in Figure 1c. From top to bottom, the histograms show data for OPV 1 (red), OPE compounds 2–4, and the two references, octanedithiols in mesitylene (black) and the solvent alone (gray). (b) A  $\log G$ -histogram of an OPV measurement that shows a fine structure (arrows) in addition to the gross Gaussian-like peak (green curve) that spans about 1 order of magnitude. In the linear  $G$ -histogram representation (c), the fine structure appears as a pair of peaks spaced by a factor of 2. Panel c also shows that the solvent alone yields a background that follows a  $1/G$  dependence (gray). For the measurement with OPE/OPV molecules, the background is deduced as a constant value at the low  $G$  side of the  $\log G$ -histogram (black horizontal line in panel b) which transforms into the  $1/G$  dependence in the  $G$ -histogram shown as a solid curve in panel c.

measurement sets into account, we can hardly resolve a difference between the three kinds of OPE molecules. We therefore conclude, that the side groups at the central phenyl ring, added to increase solubility, have no measurable effect on the electron transfer. We emphasize here that the side groups in compounds 3 and 4 do apparently not prevent the molecules from anchoring within the junction. It is also interesting to note, that the width of the molecular signature in the  $\log G$ -histograms are similar for all anchored molecules. Because of the strong difference between OPE/OPV and  $C_8$  molecules, we suggest that the width is to a great extent caused by fluctuations in the particular anchoring comprising S–Au bonds.<sup>38</sup> In addition to “bare” fluctuations leading to a wide conductance peak, a fine structure, consisting of a set of multiple peaks can be superimposed. An example for an OPV measurement is shown in Figure 2b, where the two arrows point to the fine structure. We also emphasize that the visibility of this fine structure varies from sample to sample displaying no fine structure, one, two,

(36) Costa-Kramer, J. L.; Garcia, N.; Olin, H. *Phys. Rev. Lett.* **1997**, *78*, 4990.

(37) Yasuda, H.; Sakai, A. *Phys. Rev. B* **1997**, *56*, 1069.

(38) Venkataraman, L.; Klare, J. E.; Nuckolls, C.; Hybertsen, M. S.; Steigerwald, M. L. *Nature* **2006**, *442*, 904.

and sometimes even three peaks. These “satellite” peaks are attributed to the formation of multiple molecular bridges.<sup>10,39</sup> Because the conductance value for a molecular junction consisting of  $n$ -molecules bridging the gap in parallel is expected to be  $n$ -times the single-molecule  $G$ -value, the fine structure is better analyzed in a linear representation, where multiples of a fundamental value can more easily be determined. This is illustrated in Figure 2c, where the same OPV data set as in Figure 2b is plotted. The fine structure consists in this case of two peaks, which indeed appear approximately at conductance values that agree with a single molecule junction for the lower conductance peak and a double-molecule junction for the higher one. We also plot in the same graph the tunneling background on the low- $G$  side (black curve), which follows a  $1/G$  dependence.<sup>4</sup> It can best be determined from the log  $G$ -histogram at the low- $G$  side as a constant value (shown as a black horizontal line in Figure 2b).

More explicitly, the conversion from the log  $G$ -histogram,  $N_{\log G}(\log G) = N_g(g)$ , to the linear one,  $N_G(G)$ , is given by  $N_G(G) = N_g(g)(\log(e)/G)(\Delta G/\Delta g)$ , where  $\Delta G$  and  $\Delta g$  denote the (constant) bin-size in the  $G$ - and log  $G$ -histogram, respectively (see Supporting Information). This relation transforms the shape of the molecular features in a distinct manner. The gross molecular signal, which appears as a relatively wide Gaussian-like peak in the log  $G$ -histogram is converted into a highly asymmetric peak in the linear histogram. Because of the large width of the molecular signal in the log  $G$ -histogram, which spans an order of magnitude in  $G$  values, the major contribution in the linear histogram comes from the central part where  $N_{\log G}$  is approximately constant, leading to a tail that follows approximately an  $1/G$  dependence (see dashed curve in Figure 2c and the corresponding dashed line in Figure 2b).

To quantitatively analyze our data, we proceed along two alternative methods. In method a, we base our analysis on the gross molecular signature seen in the log  $G$ -histogram. We first subtract the low- $G$  background to the left of the peak and then fit a Gauss function to the remaining peak (this procedure is highlighted with the curve in Figure 2b). To determine the center value, we first transform this Gauss function from the logarithmic to the linear representation (Supporting Information). The symmetric peak in the log  $G$ -histogram gets thereby strongly skewed. The low conductance side of the peak is compressed to values close to zero, leading to a sharp increase on the left, whereas the high conductance side is stretched into a long tail with approximate  $1/G$  dependence. This is seen in Figure 3 which shows the data of molecules 1–4 in the most interesting region in the form of a linear  $G$ -histogram for  $G$ -values in the range from  $3 \times 10^{-5}G_0$  to  $3 \times 10^{-3}G_0$ . The tunneling background, appearing at low  $G$  values (the  $1/G$  dependence shown as a solid curve in Figure 2c), has been subtracted for all set of measurements. The dashed curve represents the transformed Gaussian fits. It is quite remarkable how good this function describes the overall distribution visible in the linear  $G$ -histogram. Because of this very good agreement, we use the value  $G^a$  of the peak position of the transformed curve as a measure of the single-molecule value determined by method a. We note, that this is one particular choice. We also stress that the peaks are centered at a different position in the two kinds of histograms. The peak appears at slightly lower values in the

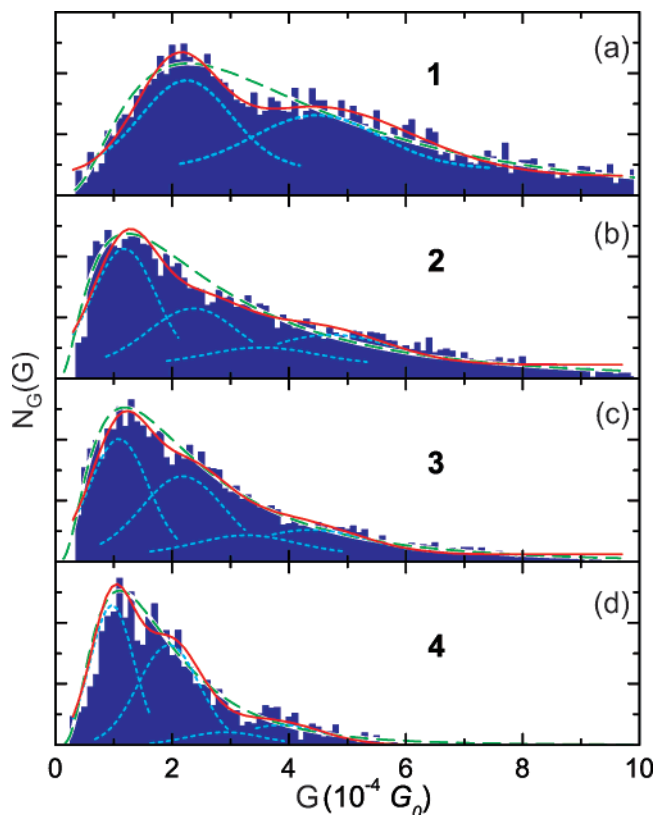


**Figure 3.** Four representative measurements of molecules 1–4 in linear-scale  $G$ -histograms with subtracted background. The dotted curves (blue) correspond to the components of the multiple Gaussian-peak fits, resulting in the solid curves (red). The dashed curves (green) have been obtained from a Gauss function fitted to the overall peak visible in log  $G$ -histogram (see for example the green curve in Figure 2b) and being then transformed onto the linear-scale  $G$ -histogram.

$G$ -histogram compared to the log  $G$  one (Figure S1, Supporting Information).

Whereas method a emphasizes the overall molecular signal visible in the log  $G$ -histogram, method b now focuses on the fine structure, which is better visible in the linear  $G$ -histograms. This second analysis assumes that the histogram is made up of contributions from junctions with one, two, or a multiple of molecules bridging the gap in parallel. We then assume that the peak positions of the fine structure occur at multiples of a fundamental value, which we term  $G^b$ . We use a multi-Gaussian fit (dotted curves in Figure 3) with up to four Gauss peaks centered at multiples of  $G^b$ . The first peak has the width  $w^b$  at half-maximum. To reduce the number of fitting parameters, we assume in addition that the width of successive peaks grows with the square-root of the number of molecules in the junction. The red solid curves in Figure 3 correspond to the result of this procedure. Owing to the large number of parameters, it is not too surprising that a good agreement results. We stress however, that independent of this procedure, major peaks are visible without applying a fitting procedure. The fitting procedure only serves to assess numbers in an objective manner.

We can now plot in Table 1 the main results, which are average single-molecule conductance values  $G^a$  and  $G^b$ , obtained by methods a and b for molecules 1–4, as well as the width at half-maximum  $w^b$ . First, it is clear that  $w^b$  is of the same size as the mean conductance value itself. Second, there is a remarkable agreement between  $G^a$  and  $G^b$  values. This coincidence is surprising and was not anticipated.

(39) Xu, B.; Tao, N. *J. Science* **2003**, *301*, 1221.

**Table 1.** Average Single-Molecule Conductance Values  $G^{a,b}$  for Molecules 1–4, Obtained with Methods a and b, Respectively<sup>a</sup>

molecule	no. of samples	$G^a$ ( $10^{-4}G_0$ )	$G^b$ ( $10^{-4}G_0$ )	$w^b$ ( $10^{-4}G_0$ )
1	5	$2.0 \pm 0.2$	$2.1 \pm 0.2$	1.7
2	5	$1.2 \pm 0.1$	$1.2 \pm 0.2$	1.1
3	4	$1.2 \pm 0.1$	$1.2 \pm 0.1$	1.1
4	3	$1.2 \pm 0.2$	$1.1 \pm 0.1$	1.0

The OPE molecules (2–4), all yield identical single-molecule conductance values of  $G_{\text{OPE}} = 1.2 \times 10^{-4}G_0$ , in good agreement with the single molecule measurements of Xiao et al.<sup>29</sup> Calculations predict however substantially larger absolute values (more than an order of magnitude) for OPE of  $2.4 \times 10^{-3}G_0$ <sup>40</sup> and  $2.1 \times 10^{-2}G_0$ .<sup>41</sup> Our comparison on the single-molecule level of OPE with OPV shows that OPV conducts slightly better. We obtain  $G_{\text{OPV}} = 2 \times 10^{-4}G_0$ , or expressed in terms of a ratio,  $G_{\text{OPV}}/G_{\text{OPE}} \approx 1.7$ . Whereas the absolute values in first principle calculations deviate substantially, one can obtain agreement in the relative numbers. Paulsson et al. have calculated the conductance values for both OPV (1) and OPE (2) and find a ratio of 1.7 between OPV and OPE, in excellent agreement with our result.<sup>41</sup> On the experimental side, our OPV value agrees with a recent AFM study on OPV molecules inserted into an alkanethiol self-assembled monolayer by Seferos et al. who reports  $15.8 \pm 6.9$  nS, which converts to  $G_{\text{OPV}} \approx 2 \times 10^{-4}G_0$ .<sup>21</sup>

We can try to explain the conductance ratio between OPV and OPEs, assuming the simplest possible model for the electron transfer, which is single-step through-molecule tunneling with a square potential-barrier determined by the highest occupied molecular orbital–lowest unoccupied molecular orbital (HOMO–LUMO) gap  $E_g$ . Then,  $G$  is given by  $G = A \exp(-2\sqrt{2\phi md}/\hbar)$ , where  $m$  is the electron mass,  $d$  the length of the molecule measured between the sulfur atoms,  $\phi$  the barrier height, assumed to be half of  $E_g$ , and  $A$  a constant determined by the Au–S bond, which should therefore be equal for all molecules. We determine an average HOMO–LUMO gap  $\bar{E}_g$  for each molecule from the optical UV–vis adsorption spectra (Figure S2, Supporting Information). We obtain  $\bar{E}_g = 3.2$  for OPV 1, 3.5 for OPE 2, for the two OPEs 3,4 with side groups (sg-OPEs). Taking OPE as our reference conductance value, this simple approach then predicts that OPV should conduct 3.6 times better, while the sg-OPEs should only conduct 1.5 times better. Here, we have used a fixed distance  $d = 2.0$  nm for all molecules. The predicted sequence, that the OPEs have similar conductance values and the OPV conducting better, is well reproduced in the experiment. We note, however, that the relaxed sulfur–sulfur distance of OPV should be slightly shorter than that of OPE. This would increase the ratio  $G_{\text{OPV}}/G_{\text{OPE}}$  to values  $>4$ . This discrepancy may be resolved if we take the

(40) Tomfohr, J.; Sankey, O. F. *J. Chem. Phys.* **2004**, *120*, 1542.(41) Paulsson, M.; Frederiksen, T.; Brandbyge, M. *Nano Lett.* **2006**, *6*, 258.

force into account which is constantly pulling on the partially flexible molecule and thereby increasing the actual distance between the terminal anchor groups, possibly in a different manner for OPE and OPV. It may also be possible that the different rigidity of the two molecules in the axial direction yields different thermal fluctuation amplitudes, affecting the average conductance values.

Finally, one cannot stress enough the uncomfortable situation that there is considerable disagreement in the conductance value of such a simple molecule as the OPE. Whereas early experiments by Reichert et al. and Mayor et al. yielded a very large conductance value of  $G_{\text{OPE}} \approx 2.5 \times 10^{-3}G_0$ ,<sup>27,28</sup> a recent single-molecule STM study reports a value of only  $2.6 \times 10^{-5}G_0$ ,<sup>31</sup> with our value  $G_{\text{OPE}} \approx 1.2 \times 10^{-4}G_0$  lying somewhere in between. Even larger values of  $G_{\text{OPE}} \approx 10^{-2}$  and  $G_{\text{OPV}} \approx 4 \times 10^{-2}G_0$  were reported by Kusmerick et al.<sup>22</sup> using crossed-wire junctions. In this latter case it is however likely that many molecules were measured in parallel.

In conclusion, we have compared the molecular signature of four different conjugated molecules in break junctions at the single molecule level and under identical environmental conditions. We find a larger conductance value of  $2 \times 10^{-4}G_0$  for OPV as compared to three OPE compounds, which all show a conductance of  $1.2 \times 10^{-4}G_0$ . Our data suggest that the three phenyl rings are close to planar, even in the presence of the solubilizing side groups, maximizing the conjugation. We have also put forward a new method to analyze conductance values  $G$  based on a histogram of the logarithm of  $G$ . In such a histogram all the weight that can be assigned to the presence of molecules anchoring in the gap yields a symmetric peak, whereas the data in a linear  $G$  representation is a strongly asymmetric peak that assumes a power-law dependence over almost the whole range of  $G$ -values, closely following a  $1/G$ .

**Acknowledgment.** We acknowledge fruitful discussion with M. Brandbyge and N. J. Tao. T.G. thanks the “Ministerio de Educación y Ciencia” and the “Freie Akademische Gesellschaft” (FAG) for financial support; C.W. thanks EPSRC (U.K.) for funding; R.J. thanks the Royal Thai Government for the award of a scholarship. This work has been supported by the Swiss NSF through the NCCR “Nanoscale Science” and the Eurocores Programme SONS.

**Supporting Information Available:** Derivation of the transformation between the logarithmic and linear histogram; UV–vis adsorption spectra of the molecules. This material is available free of charge via the Internet at <http://pubs.acs.org>. <sup>a</sup>Whereas  $G^a$  is deduced from fits to the overall peak in the log  $G$ -histograms,  $G^b$  focuses on the fine structure which is better visible in the linear  $G$ -histograms. In addition, the full-width at half-maximum  $w^b$  of the single-molecule peak obtained from the linear histograms is given as well. All numbers show a higher  $G$ -value for OPV than OPE.

JA0767940

## Supporting Information

# Electrical conductance of conjugated oligomers at the single molecule level

Roman Huber<sup>1</sup>, Maria Teresa González<sup>1</sup>, Songmei Wu<sup>1</sup>, Michael Langer<sup>2</sup>, Sergio Grunder<sup>2</sup>, Viviana Horhoiu<sup>2</sup>, Marcel Mayor<sup>2,3</sup>, Martin Bryce<sup>4</sup>, Changsheng Wang<sup>4</sup>, Rukkiat Jitchati<sup>4</sup>, Christian Schönenberger<sup>1\*</sup>, and Michel Calame<sup>1\*</sup>

<sup>1</sup>*Department of Physics, University of Basel, Klingelbergstrasse. 82, CH-4056 Basel, Switzerland*

<sup>2</sup>*Department of Chemistry, University of Basel, St. Johanns-Ring 19, CH-4056 Basel, Switzerland*

<sup>3</sup>*Forschungszentrum Karlsruhe GmbH, Institute for Nanotechnology, P.O. Box 3640, D-76021 Karlsruhe, Germany*

<sup>4</sup>*Department of Chemistry, University of Durham, Durham DH1 3LE, UK*

E-mail: christian.schoenenberger@unibas.ch, michel.calame@unibas.ch

## Transformation between the logarithmic and linear histogram

In the first part of this supporting information we derive the transformation between the *logarithmic* and *linear* histogram, which we have used in the main text for the presentation of the measured electrical conductance values  $G$ .

Histograms are constructed from a set of measured conductance values  $G_{j,i}^{><} = G_j^{><}(z_i)$ , acquired repetitively (index  $j$ ) during opening ( $>$ ) and closing ( $<$ ) of the junctions.  $z_i$  denotes the pushrod position at the instance of a measurement, acquired and stored in the computer. Because we only focus on the dependence of  $G$  while opening the junction in this work, we disregard  $G^{<}$  in the following. Furthermore, we will also assume that the successive  $z$ -values, i.e.  $z_i, z_{i+1}$ , are lying so dense that a continuum approximation is justified. We introduce the abbreviation  $g = \log(G)$  and  $N_{tot}$  for the total number of points entering both the  $G$  and  $\log G$ -histogram.

Let  $p_G(G)$  denote the probability to measure a conductance value in the interval  $G \dots G + dG$ , and similarly  $p_g(g)$  the probability to measure a  $g$ -value in the interval  $g \dots g + dg$ . Then, the relation

$$p_G(G)dG = p_g(g)dg \quad (1)$$

holds. Because  $g = \log(G)$ , it further follows that

$$dg = d(\log G) = \log(e)d(\ln G) = \log(e)\frac{dG}{G}. \quad (2)$$

Taking eq 1 and eq 2, yields the relation

$$p_G = p_g \log(e)/G. \quad (3)$$

If we denote with  $\Delta G$  and  $\Delta g$  the respective bin-widths of the linear and log-histogram, the linear  $N_G(G)$  and the log-histogram  $N_g(g)$  are defined by:

$$N_G(G) = N_{tot} p_G(G) \Delta G \quad (4)$$

$$N_g(g) = N_{tot} p_g(g) \Delta g \quad (5)$$

Replacing  $p_G$  in eq 4 with eq 3 and combining with eq 5, yields the final result:

$$N_G(G) = N_g(\log G) \frac{\log(e)}{G} \frac{\Delta G}{\Delta g}. \quad (6)$$

This equation shows that if the log-histogram  $N_g(g)$  is constant, the linear histogram  $N_G(G)$  is proportional  $1/G$ .<sup>1</sup>

In the paper, we also show that the molecular signal in the  $\log G$ -histogram can be approximated by a Gauss function, i.e. we fit  $N_g(g)$  according to:

$$N_g(g) = C \exp\left(-\frac{(g - g_c)^2}{2w_g^2}\right), \quad (7)$$

where  $w_g$  denotes the width,  $g_c$  the center value, and  $C$  a constant. This Gauss function is transformed into the linear  $G$ -histogram, using eq 6, i.e.:

$$N_G(G) \propto \frac{\exp\left(-\frac{(\log G - g_c)^2}{2w_g^2}\right)}{G}. \quad (8)$$

This transformation is explicitly illustrated in Fig. S1. The position of the maximum in the  $\log G$ -histogram is by definition  $g_c$ . After the transformation to the linear histogram, the peak position is however not found at the value  $G_C = 10^{g_c}$ , but it is shifted to a lower value, given by:

$$\log(G_c) = g_c - \ln(10)w_g^2. \quad (9)$$

This can be derived by setting the derivative of eq 8 to zero and solving for  $\log G$ .

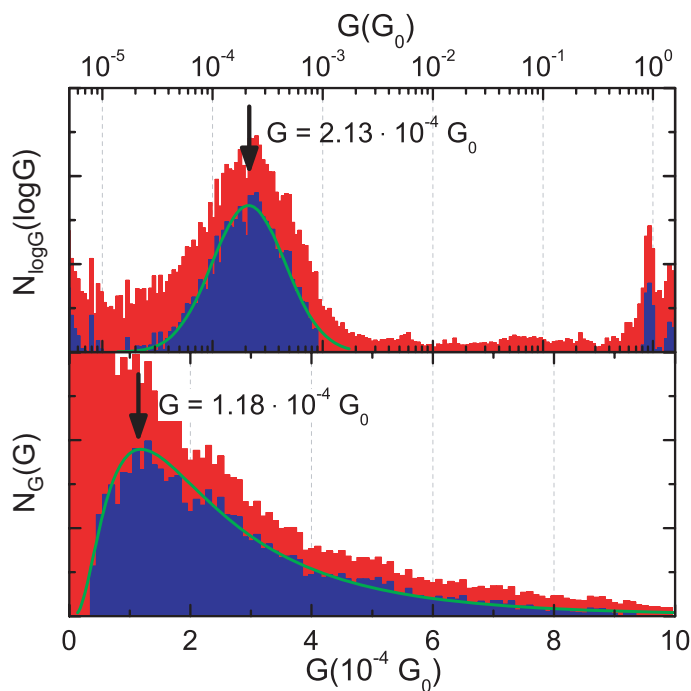


**Figure S1.** (a) Log plot of a measurement of **2** including the fitted Gauss curve having the width  $w_g = 0.33$ , and a peak maximum appearing at  $2.13 \cdot 10^{-4}G_0$ . The horizontal line shows the subtracted background. (b) linear plot of the same data, including the transformed Gauss function as described in the text. The maximum is shifted to the left, located at  $1.18 \cdot 10^{-4}G_0$ .

### HOMO-LUMO gaps from optical UV-vis adsorption spectra

Figure S2 shows the UV-vis adsorption spectra of compounds **1-4** measured in dichlormethane. It is seen that the spectrum of OPV looks remarkably similar to the one of OPE, except that the former is red-shifted by  $\approx 30$  nm, due to the higher conjugation of the pi-electron system in OPV.

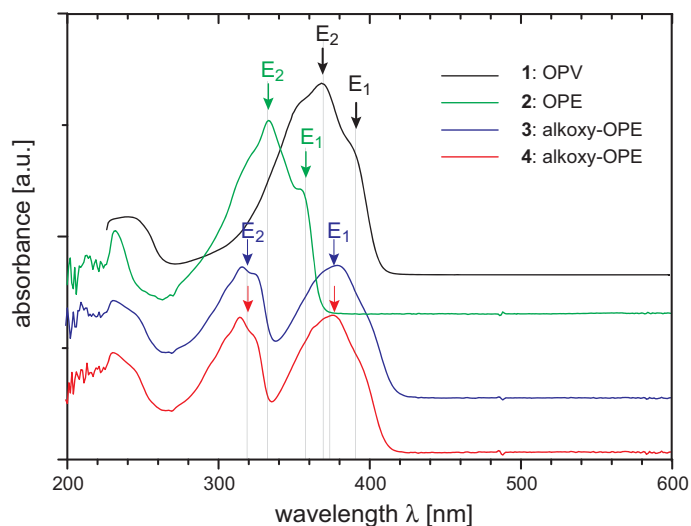


**Figure S2.** UV-vis adsorption spectra of compounds **1-4** measured in dichloromethane.

The OPE molecules with alkoxy substitutions in the 2,5 position of the central phenyl ring display a different adsorption spectrum. Whereas for OPV and OPE two peaks overlap, which are visible as a dominant peak and a weaker shoulder at longer wavelength, the two peaks markedly split apart for the modified OPEs. This has been described in the work of James *et al.*<sup>2</sup> who assigned the peaks to two close-lying HOMO orbitals.

To deduce an effective HOMO-LUMO gap  $E_g$  for the electron transfer, we determine the energies  $E_{1,2}$  of both transitions (arrows) from the wavelengths  $\lambda_{1,2}$  at the center of the peaks. We assume that the electron transfer probability is given by  $T(E_g) = A \exp(-2\sqrt{m\overline{E}_g}d/\hbar)$  with a constant  $A$ , meaning that both orbitals couple equally to the electrodes. The average gap  $\overline{E}_g$  is then obtained from the following equation:  $T(\overline{E}_g) = (T(E_{g1}) + T(E_{g2}))/2$ . This yields the values 3.5, 3.2, and 3.44 eV for molecules **1-3**, respectively. Molecule **4** is identical to molecule **3**.

## References

- (1) González, M. T.; Wu, S.; Huber, R.; van der Molen, S. J.; Schönenberger, C.; Calame, M. *Nano Letters* **2006**, *6*, 2238.
- (2) James, P. V.; Sudeep, P. K.; Suresh, C. H.; Thomas, K. G. *J. Phys. Chem. A* **2006**, *110*, 4329.